Influence of interlayer stacking arrangements on carrier accumulation in bilayer graphene field effect transistors

Yanlin Gao,* Mina Maruyama,† and Susumu Okada‡

Department of Physics, Graduate School of Pure and Applied Sciences, University of Tsukuba, 1-1-1 Tennodai, Tsukuba, Ibaraki 305-8571, Japan

Abstract

The electronic structure of bilayer graphene under an external electric field is studied in terms of the interlayer stacking arrangements using the density functional theory combined with the effective screening medium method. The calculations showed that the accumulated carrier distribution strongly depended on the interlayer stacking arrangement. The carriers were highly concentrated on the topmost layer of twisted bilayer graphene, while carriers were also found in the second layer of bilayer graphene with the AA and AB interlayer arrangements. In addition to the carrier accumulation, ab initio molecular dynamics calculations also revealed that the interlayer Seebeck coefficient and thermal diffusivity in the bilayer graphene depended on the interlayer stacking arrangements.

Following the synthesis of graphene [1–5], graphene has attracted much attention in the field of low-dimensional science and nanotechnology [6, 7]. Its honeycomb covalent network of carbon atoms endows graphene with a semiconducting electronic structure with a vanishing density of states at the Fermi level because of the conical dispersion band around the K point [8–10]. This electronic band structure leads to an unusual quantum Hall effect and results in remarkable carrier mobility of a few hundred thousand cm^2/Vs [11–13], making graphene a unique and emerging material in the wide area of pure and applied sciences. Because of its sheet structure with single-atom thickness and peculiar electronic structure, graphene is regarded as an emerging material for various devices in the near future, such as sensing devices, semiconducting devices, and transparent electrodes. However, difficulties exist in device fabrication processes owing to the fragility of the electronic properties of graphene in devices.

Graphene can be used as a starting material for designing other nanoscale low-dimensional materials with unusual physical properties by controlling their dimensionality, size, and shape [14–18]. Large-area graphene occasionally possesses grain boundaries at which topological defects are formed owing to the lattice misorientation between adjacent grains [19]. These grain boundaries cause unusual localized states around them that depend on the constituent polygons and their arrangements at the boundaries [20]. Graphene is known to form in-plane heterostructures with h-BN possessing zigzag borders consisting of BC bonds [21–28], which induce the border localized states [29–31]. In addition to these in-plane heterostructures, graphene can also form out-of-plane structures with other graphene layers or with other two-dimensional materials such as h-BN and transition metal dichalcogenides, because of their chemically inert surfaces [32–34]. Bilayer graphene and few-layer graphene are representative examples of such out-of-plane structures, exhibiting interesting electronic structure variations that are highly dependent on the interlayer stacking arrangement [35]. Bilayer graphene with an AB stacking arrangement possesses parabolic bands at the Fermi level, while that with an AA stacking arrangement has two conical bands below and above the Fermi level [8, 35, 36]. Furthermore, a Fermi level velocity deceleration has been observed in bilayer graphene possessing a twisted interlayer arrangement, leading to unusual physical phenomena [37–39].

Field effects on the electronic properties of graphene thin films are an important subject for practical application of these thin films. Experimental and theoretical works demonstrate

that an electric field modulate the electronic structure of graphene thin films [36, 40–43]. A perpendicular electric field induces a finite band gap in bilayer graphene with the AB interlayer arrangement, where the width of the band gap depends on the field strength [36]. Bilayer graphene with twisted arrangement in a particular mutual angle (i.e., twisted bilayer graphene) exhibits superconductivity under carrier doping via an electric field [39]. Magnetic states on the (111) surfaces of rhombohedral graphene thin films (i.e., graphene thin films with ABC interlayer arrangement) are tunable by the film thickness and a perpendicular electric field [41–43]. Although these works indicate that the electronic structure and carrier distribution of graphene thin films under an electric field depend on the mutual stacking arrangement, the detailed correlation between the electronic properties and the stacking arrangement in graphene thin films under a normal electric field remains unclear. Therefore, in this work, we aim to provide theoretical insight into the influence of the interlayer stacking arrangement on the electronic structure of bilayer graphene, performing first-principles total energy calculations combined with the effective screening medium method (ESM) . Our calculations show that the carriers are extended throughout the layers for graphene with the AB arrangement. Conversely, the carriers are highly localized on the layer situated at the electrode side for twisted bilayer graphene. In addition to the electronic structure, the thermal and thermoelectric properties of bilayer graphene is also found to depend on the stacking arrangement.

All calculations were performed within the framework of density functional theory [44, 45] implemented in a STATE package [46]. We used the generalized gradient approximation with the Perdew-Burke-Ernzerhof functional [47, 48] to describe the exchange-correlation potential energy among interacting electrons. The weak dispersive interaction between graphene layers was treated using the vdW-DF2 with the C09 exchange-correlation functional [49, 50]. An ultrasoft pseudopotential generated by the Vanderbilt scheme was used to describe the interaction between electrons and ions [51]. The valence wave functions and deficit charge density were expanded in terms of the plane-wave basis set with cutoff energies of 25 and 225 Ry, respectively. We adopted the ESM to solve the Poisson equation including an external electric field [52]. The Brillouin-zone integration was performed with the $50\times50\times1$ and $14\times14\times1$ $\boldsymbol{k}$-meshes for self-consistent electronic structure calculations of bilayer graphene with AB(AA) and twisted interlayer arrangements, respectively. All atoms were fully optimized until the remaining force acting on each atom was less than 0.005 Ry/Å under a fixed

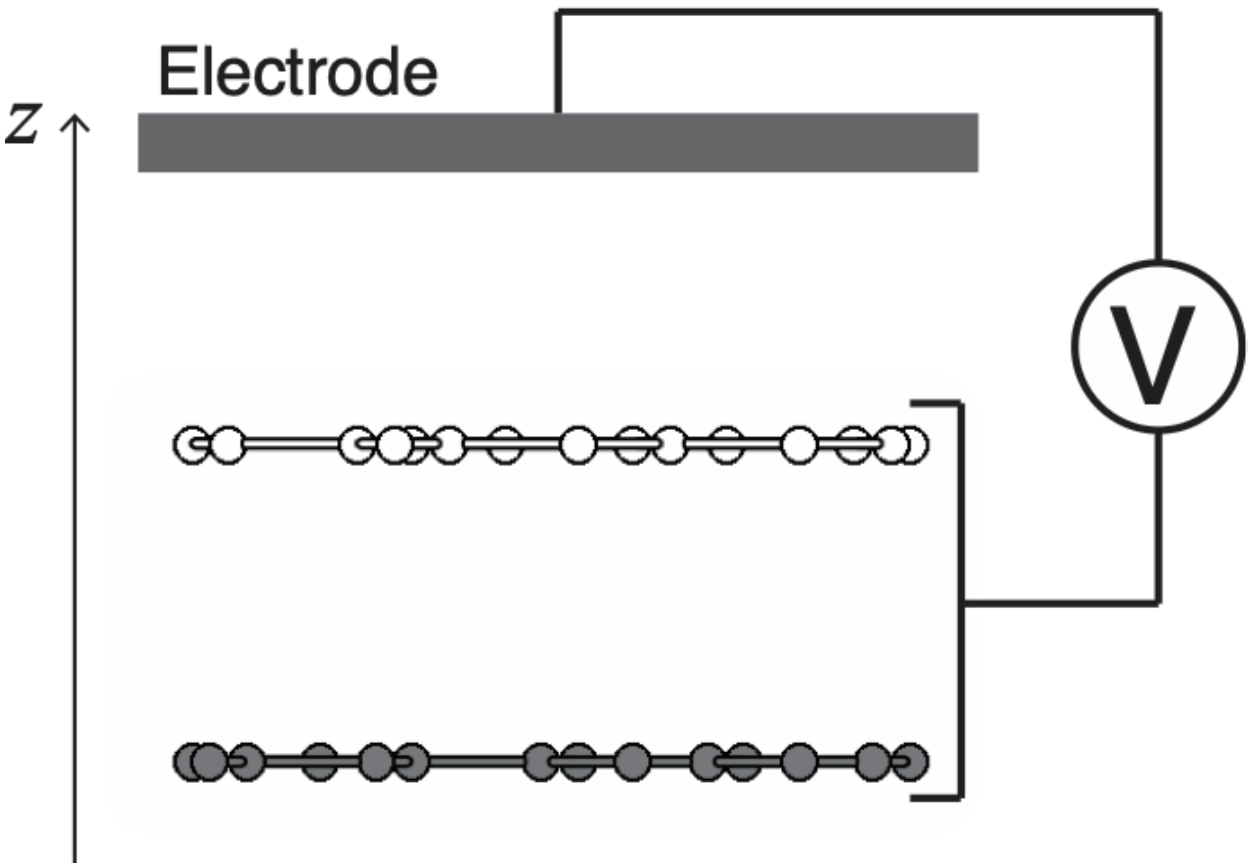

FIG. 1. (a) Structural model of bilayer graphene in a single-gate field effect transistor. (b) Geometric structure of twisted bilayer graphene with a twist angle of $\theta = 28°$. gray rectangular indicate the metal electrode with the infintite permittivity simulated by the effective screening medium. White and gray circles denote C atoms belong to the topmost and second layers of bilayer graphene, respectively. Gray quadrangle indicate the lateral unit cell of the twisted bilayer graphene.

lateral lattice constant of 2.4595 Å, which corresponds to the experimental value.

In the present work, we considered bilayer graphene with AB, AA, and twisted interlayer arrangements. For the twisted interlayer arrangement, we considered twisted bilayer graphene with a twist angle of $\theta = 28°$. During the calculations under a finite electric field, we assumed that the atomic structure of the bilayer graphene was fixed at the optimized structure obtained under zero electric field. Electrons and holes were injected by a planar electrode situated above the bilayer graphene with a vacuum spacing of 5.0 Å, mimicking the single-gate graphene field effect transistor (FET) shown in Fig. 1. The electrode was simulated using an effective screening medium with an infinite relative permittivity. To

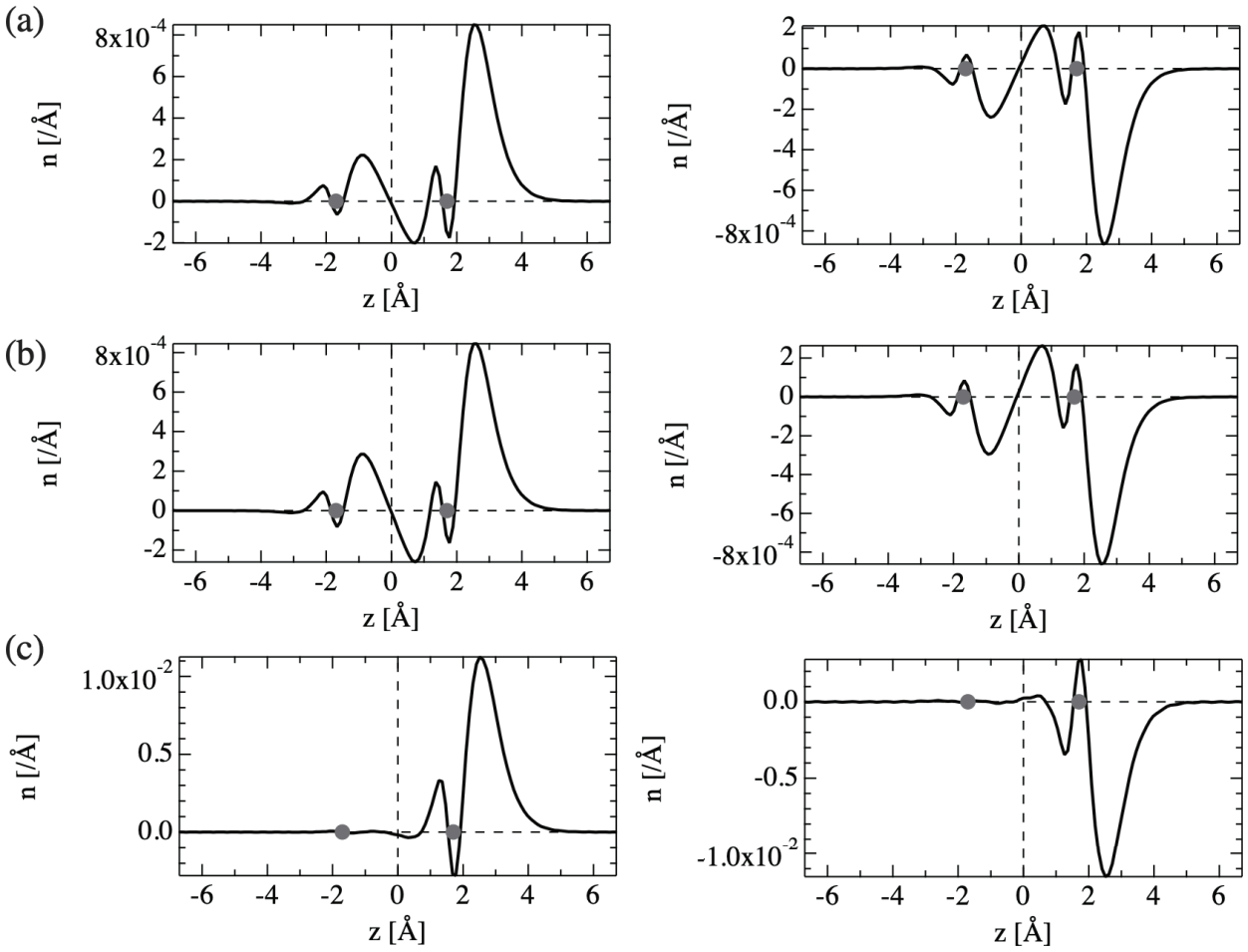

FIG. 2. Charge densities normal to the bilayer graphene with (a) AB, (b) AA, and (c) twisted interlayer arrangements under an electric field, showing the charge densities under electron doping (left plots) and hole doping (right plots). Gray circles denote the atomic position of bilayer graphene.

analyze the thermoelectric and thermal properties of the bilayer graphene in terms of the stacking arrangements, we considered bilayer graphene with AB and twisted ($\theta = 28°$) interlayer arrangements that possessed the same lateral unit cell. This enabled a quantitative discussion of the Seebeck coefficient and the thermal diffusivity between layers in terms of the stacking arrangement. An open boundary condition along the direction normal to the graphene layer was imposed by putting an effective screening medium with $\varepsilon_r = 1$ at the cell boundaries.

Figure 2 shows the carrier distribution across the graphene layer under excess carriers of

0.19e(h)/nm^2. The carrier distribution $n(z)$ is evaluated by

$$n(z) = \int \{\rho_F(\boldsymbol{r}) - \rho_0(\boldsymbol{r})\} dxdy$$

where $\rho_F(\boldsymbol{r})$ and $\rho_0(\boldsymbol{r})$ are electron density with and without external electric field. It is seen that the distribution of accumulated carriers in bilayer graphene under an external electric field strongly depends on the interlayer stacking arrangement. For the AB stacking under electron doping, 80% of doped electrons are accommodated in the topmost layer, while 20% are on the second layer. Accumulated holes exhibit a similar distribution: 79 and 21% of the doped hole are distributed on the topmost and second layers, respectively, under a perpendicular electric field, indicating an electron-hole symmetry for the carrier doping [Fig. 2(a)]. The penetration of injected carriers increases in the AA stacking arrangement, where 74 and 26% of carriers are distributed in the topmost and the second layers of graphene, respectively, irrespective of the carrier species [Fig. 2(b)]. This large carrier penetration into the second layer is ascribed to hybridization of the interlayer wavefunction, where the wavefunction hybridization in AA graphene is larger than that in AB graphene owing to the perfectly overlapped interlayer atomic arrangement of the former. These results imply that the carrier is highly concentrated in the first layer of the twisted bilayer graphene because of its weak interlayer wavefunction coupling. Indeed, the carrier distribution is highly concentrated in the topmost layer of the twisted bilayer graphene for both electron and hole doping [Fig. 2(c)], as in the case for a bilayer transition metal dichalcogenide with a twisted arrangement under a normal electric field [53]. By integrating the accumulated carriers along the z axis, carriers are perfectly localized on the topmost layer for electron and hole doping cases. Therefore, the stacking misorientation can control the carrier penetration depth in graphene thin film FETs.

The accumulated carrier distribution causes a variation in the capacitance of the bilayer graphene FET in terms of the stacking arrangement. Figure 3 shows the capacitance of the bilayer graphene FET with a single top gate electrode. The capacitance C is evaluated by calculating $q/V_{\rm G}$ where q is the carriers injected by the electrode and $V_{\rm G}$ is the corresponding gate voltage with respect to the vacuum level situated at the opposite cell boundary to the gate electrode. The capacitance is found to depend on the stacking arrangement. For bilayer graphene with AB and AA arrangements, the capacitance weakly depends on the gate voltage [Figs. 3(a) and 3(b)], where the capacitance of the AA arrangement is slightly

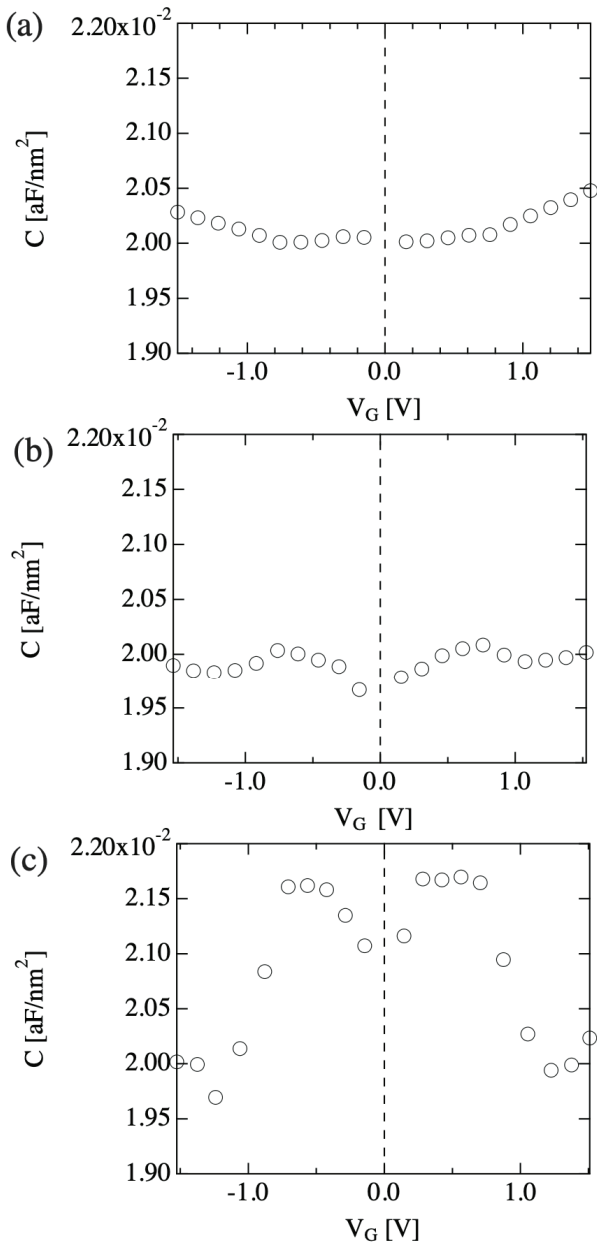

FIG. 3. Capacitance of bilayer graphene with (a) AB, (b) AA, and (c) twisted interlayer arrangements. Positive and negative V_G correspond to electron and hole doping, respectively.

lower than that of the AB arrangement. This lower capacitance may relate to the lower carrier concentration on the topmost layer in the bilayer graphene with the AA stacking. In contrast, the capacitance of the twisted bilayer graphene is higher than that of the other two bilayer graphene and exhibits a relatively large gate voltage dependence.

We also investigated the electrostatic potential normal to the graphene layers under an

electric field corresponding to a carrier density of 0.19e(h)/nm^2 (Fig. 4). The potential drop mainly occurs between the topmost layer and the electrode, because the majority of carriers are accommodated in the topmost layer. Careful analysis of the potential between the layers reveals that the electric field between the layers depends on the stacking arrangements. Specifically, the electric field values for electron and hole doping at the middle of the bilayer graphene with AB stacking are 0.68 and 0.71 V/nm, respectively, which is the smallest values among the bilayer graphene studied here [Fig. 4(a)]. The electric field values for electron and hole doping between the layers of bilayer graphene with AA stacking is 0.88 and 0.83 V/nm, respectively [Fig. 4(b)]. These large electric field values are ascribed to the strong interlayer dipole associated with the carriers induced on the second layer and in the interlayer vacuum spacing [Fig. 4(b)]. The twisted arrangement also induces large electric field values for electron and hole doping at the middle of the layers of 0.80 and 0.83 V/nm, respectively [Fig. 4(c)]. Unlike the case with the AA arrangement, the carrier concentration in the topmost layer of the twisted bilayer graphene leads to the large potential difference between the layers.

Next, we determine the modulation of the electronic energy band via the carrier injection (Fig. 5). For the AB arrangement, both electron and hole injections cause a finite energy gap between the valence and conduction bands at the vicinity of the K point, owing to the electrostatic potential difference between layers and the band repulsion [Fig. 5(a)]. However, the dispersion relation of the lowest and the highest branches of the conduction and valence bands, respectively, is different from those of the bilayer graphene with AB arrangement under the normal external electric field without excess carriers. In contrast, bilayer graphene with AA and twisted arrangements do not exhibit a substantial electronic band structure modulation under an external electric field, excepting an energy shift upon carrier injection. In particular, the band dispersion relation near the Fermi level of the bilayer graphene with AA arrangement perfectly retains the features without an external electric field. For the twisted bilayer graphene, the electron and hole injections cause the Dirac cone to split into upper and lower branches owing to the electrostatic potential difference between the layers.

Finally, the thermoelectric and thermal properties between layers of bilayer graphene in terms of stacking arrangement is ascertained via ab-initio molecular dynamics simulations. To apply a temperature difference between the layers, the initial velocities of atoms belonging to one of two layers were set to correspond to a temperature of 1000K. Then, the

electrostatic potential difference between two cell boundaries was monitored and the average atomic velocities were obtained during the molecular dynamics simulations under a constant volume and temperature of 300K. The calculated Seebeck coefficient for the AB and twisted bilayer graphene was found to be 12.01 and 12.76 μV/K, respectively. Further, the AB and twisted bilayer graphene exhibited a thermal diffusivity of 2.23×10^{-8} and 1.18×10^{-8} m^2/sec, respectively. The larger interlayer Seebeck coefficient and smaller interlayer thermal diffusivity found in the twisted bilayer graphene are ascribed to its weaker interlayer coupling compared with that in the AB bilayer graphene.

Based on DFT combined with the ESM, the electronic structure of bilayer graphene was studied in the FET structure under an electric field for various interlayer stacking arrangements. The distribution of accumulated carriers in bilayer graphene under an external electric field strongly depended on the interlayer stacking arrangement. Specifically, the carrier distribution was highly concentrated in the topmost layer of twisted bilayer graphene for both electron and hole doping. However, substantial carrier penetration was found in the second layer of AB and AA bilayer graphene, reflecting the interlayer wavefunction hybridization of these arrangements. The accumulated carrier distribution also caused an interlayer stacking dependence of the capacitance of a bilayer graphene FET. The capacitance was sensitive and insensitive to the gate voltage for bilayer graphene with and without a stacking misorientation, respectively. The carrier injection caused a large and small band structure modulation for AB and twisted bilayer graphene, respectively, owing to the electrostatic potential difference between the layers. In contrast, the field did not affect the electronic structure of AA bilayer graphene. In addition to the carrier accumulation by the external field, we investigated the interlayer Seebeck coefficient and thermal diffusivity of bilayer graphene by conducting ab-initio molecular dynamics simulations. The calculated Seebeck coefficients of the AB and twisted bilayer graphene were 12.01 and 12.76 μV/K, respectively. The AB and twisted bilayer graphene had a thermal diffusivity of 2.23×10^{-8} and 1.18×10^{-8} m^2/sec, respectively. These results indicate that the interlayer stacking arrangement crucially affects the physical properties of bilayer graphene in both electronic and thermal viewpoints.

The author thanks JST-CREST Grant Numbers JPMJCR1532 and JPMJCR1715 from the Japan Science and Technology Agency, JSPS KAKENHI Grant Numbers JP17H01069, JP16H00898, and JP16H06331 from the Japan Society for the Promotion of Science, the

Joint Research Program on Zero-Emission Energy Research, Institute of Advanced Energy, Kyoto University, and University of Tsukuba Basic Reseach Support Program (S). Part of the calculations was performed on an NEC SX-Ace at the Cybermedia Center at Osaka University.

---

* E-mail address: ylgao@comas.frsc.tsukuba.ac.jp

† E-mail address: mmaruyama@comas.frsc.tsukuba.ac.jp

‡ E-mail address: sokada@comas.frsc.tsukuba.ac.jp

[1] K. S. Novoselov, A. K. Geim, S. V. Morozov, D. Jiang, Y. Zhang, S. V. Dubonos, I. V. Grigorieva, and A. A. Firsov, Science **306**, 666 (2004).

[2] A. K. Geim and K. S. Novoselov, Nat. Mater. **6**, 183 (2007).

[3] I. Forbeaux, J.-M. Themlin, and J.-M. Debever, Phys. Rev. B **58**, 16396 (1998).

[4] C. Berger, Z. Song, X. Li, X. Wu, N. Brown, C. Naud, D. Mayou, T. Li, J. Hass, A. N. Marchenkov, E. H. Conrad, P. N. First, and W. A. de Heer, Science **312**, 1191 (2006).

[5] X. Li, W. Cai, J. An, S. Kim, J. Nah, D. Yang, R. Piner, A. Velamakanni, I. Jung, E. Tutuc, S. K. Banerjee, L. Colombo, and R. S. Ruoff, Science **324**, 1312 (2009).

[6] M. S. Dresselhaus and G. Dresselhaus, Adv. Phys. **30**, 139 (1981).

[7] A. H. Castro Neto, F. Guinea, N. M. R. Peres, K. S. Novoselov, and A. K. Geim, Rev. Mod. Phys. **81**, 109 (2009).

[8] G. S. Painter and D. E. Ellis, Phys. Rev. **1**, 4747 (1970).

[9] F. Bassani and G.P. Parravicini, Nuovo Cimento B **50**, 95 (1967).

[10] M. Posternak, A. Baldereschi, A. J. Freeman, E. Wimmer and M. Weinert, Phys. Rev. Lett. **50**, 761 (1983).

[11] K. S. Novoselov, A. K. Geim, S. V. Morozov, D. Jiang, M. I. Katsnelson, I. V. Grigorieva, S. V. Dubonos, and A. A. Firsov, Nature **438**, 197 (2005).

[12] Y. Zhang, Y.-W. Tan, H. L. Stormer, and P. Kim, Nature **438**, 201 (2005).

[13] K. I. Bolotin, K. J. Sikes, Z. Jiang, M. Klima, G. Fudenberg, J. Hone, P. Kim, and H. L. Stormer, Solid State Commun. **146**, 351 (2008).

[14] H. W. Kroto, J. R. Heath, S. C. O'Brien, R. F. Curl, and R. E. Smalley, Nature **318**, 162 (1985).

[15] S. Iijima, Nature **354**, 56 (1991).

[16] M. Fujita, K. Wakabayashi, K. Nakada, and K. Kusakabe, J. Phys. Soc. Jpn. **65**, 1920 (1996).

[17] K. Nakada, M. Fujita, G. Dresselhaus, and M. S. Dresselhaus, Phys. Rev. B **54**, 17954 (1996).

[18] M. Maruyama and S. Okada, Carbon **125**, 530 (2017).

[19] J. Lahiri, Y. Lin, P. Bozkurt, I. I. Oleynik, and M. Batzill, Nat. Nanotechnol. **5**, 326 (2010).

[20] S. Okada, T. Kawai, and K. Nakada, J. Phys. Soc. Jpn. **80**, 013709 (2011).

[21] S. M. Kim, A. Hsu, P. T. Araujo, Y.-H. Lee, T. Palacios, M. Dresselhaus, J.-C. Idrobo, K. K. Kim, and J. Kong, Nano Lett. **13**, 933-941 (2013).

[22] J. Park, J. Lee, L. Liu, K. W. Clark, C. Durand, C. Park, B. G. Sumpter, A. P. Baddorf, A. Mohsin, M. Yoon, G. Gu, and A.-P. Li, Nat. Commun. **5**, 5403 (2014).

[23] C. Tönshoff, M. Müller, T. Kar, F. Latteyer, T. Chassé, K. Eichele, and H. F. Bettinger, Chem. Phys. Chem. **13**, 1173-1181 (2012).

[24] C. Sánchez-Sánchez, S. Brüller, H. Sachdev, K. Müllen, M. Krieg, H. F. Bettinger, A. Nicolaï, V. Meunier, L. Talirz, R. Fasel, and P. Ruffieux, ACS N ano **9**, 9228-9235 (2015).

[25] T. Gao, X. Song, H. Du, Y. Nie, Y. Chen, Q. Ji, J. Sun, Y. Yang, Y. Zhang, and Z. Liu, Nat. Commun. **6** 6835 (2015).

[26] L. Ci, L. Song, C. Jin, D. Jariwala, D. Wu, Y. Li, A. Srivastava, Z. F. Wang, K. Storr, L. Balicas, F. Liu, and P. M. Ajayan, Nat. Mater. **9**, 430-435 (2010).

[27] Y. Gao, Y. Zhang, P. Chen, Y. Li, M. Liu, T. Gao, D. Ma, Y. Chen, Z. Cheng, X. Qiu, W. Duan, and Z. Liu, Nano Lett. **13**, 3439-3443 (2013).

[28] E. Maeda, Y. Miyata, H. Hibino, Y. Kobayashi, R. Kitaura, and H. Shinohara, Appl. Phys. Express **10**, 055102 (2017).

[29] S. Okada, M. Igami, K. Nakada, and A. Oshiyama, Phys. Rev. B **62**, 9896 (2000).

[30] S. Okada and A. Oshiyama, Phys. Rev. Lett. **87**, 146803 (2001).

[31] H. Sawahata, A. Yamanaka, M. Maruyama, and S. Okada Appl. Phys. Express **11**, 065201 (2018).

[32] A. K. Geim and I. V. Grigorieva, Nature **499**, 419 (2013).

[33] K. Kim, M. Yankowits, B. Fallahazad, S. Kang, H. C. P. Movva, S. Huang, S. Larenris, C. M. Corbet, T. Taniguchi, K. Watanabe, S. K. Banerjee, B. J. LeRoy, and E. Tutuc, Nano Lett. **16**, 1989 (2016).

[34] S. Masubuchi, M. Morimoto, S. Morikawa, M. Onodera, Y. Asakawa, K. Watanabe, T.

Taniguchi, and T. Machida, Nat. Commun. **9**, 1413 (2018).

[35] M. Koshino and T. Ando, Phys. Rev. B **76**, 085425 (2007).

[36] S. Konabe and S. Okada, J. Phys. Soc. Jpn. **81**, 113702 (2012).

[37] E. Suárez Morell, J. D. Correa, P. Vargas, M. Pacheco, and Z. Barticevic, Phys. Rev. B **82**, 121407(R) (2010).

[38] R. Bistritzer and A. H. MacDonald, Proc. Natl. Acad. Sci. **108**, 12233 (2011).

[39] Y. Cao, V. Fatemi, S. Fang, K. Watanabe, T. Taniguchi, E. Kaxiras, and P. Jarillo-Herrero, Nature **556**, 43 (2018).

[40] M. F. Craciun, S. Russo, M. Yamamoto, J. B. Oostinga, A. F. Morpurgo, and S. Tarucha, Nat. Nanotechnol. **4**, 383 (2009).

[41] M. Otani, M. Koshino, Y. Takagi, S. Okada, Phys. Rev. B **81**, 161403 (R) (2010).

[42] M. Otani, Y. Takagi, M. Koshino, S. Okada, Appl. Phys. Lett. **96**, 242504 (2010).

[43] N. T. Cuong, M. Otani, and S. Okada, Surf. Sci. **606**, 253 (2012).

[44] P. Hohenberg and W. Kohn, Phys. Rev. **136**, B864 (1964).

[45] W. Kohn and L. J. Sham, Phys. Rev. **140**, A1144 (1965).

[46] Y. Morikawa, K. Iwata, and K. Terakura, Appl. Surf. Sci. **169-170**, 11 (2001).

[47] J. P. Perdew, K. Burke, and M. Ernzerhof, Phys. Rev. Lett. **77**, 3865 (1997).

[48] J. P. Perdew, K. Burke, and M. Ernzerhof, Phys. Rev. Lett. **78**, 1396 (1997).

[49] K. Lee, É. D. Murray, L. Kong, B. I. Lundqvist, and D. C. Langreth, Phys. Rev. B **82**, 081101(R) (2010).

[50] V. R. Cooper, Phys. Rev. B **81**, 161104(R) (2010).

[51] D. Vanderbilt, Phys. Rev. B **41**, 7892 (1990).

[52] M. Otani and O. Sugino, Phys. Rev. B **73**, 115407 (2006).

[53] M. Maruyama and S. Okada, Appl. Phys. Express **12**, 075008 (2019).

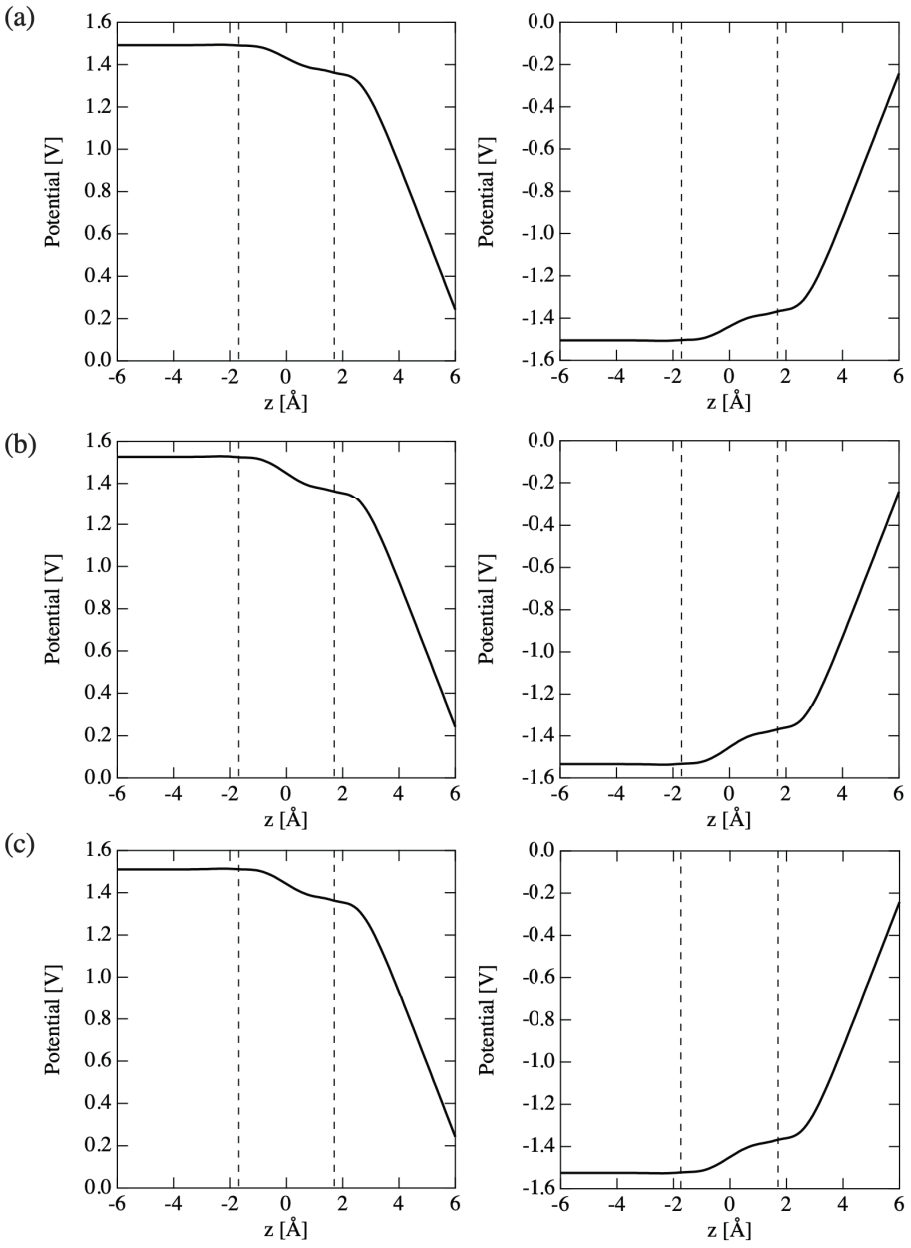

FIG. 4. Electrostatic potential normal to the bilayer graphene with (a) AB, (b) AA, and (c) twisted interlayer arrangements under an electric field corresponding to a carrier density of 0.19e(h) /nm^2, showing the potential under electron doping (left plots) and hole doping (right plots). Dotted vertical lines indicate the position of graphene layers.

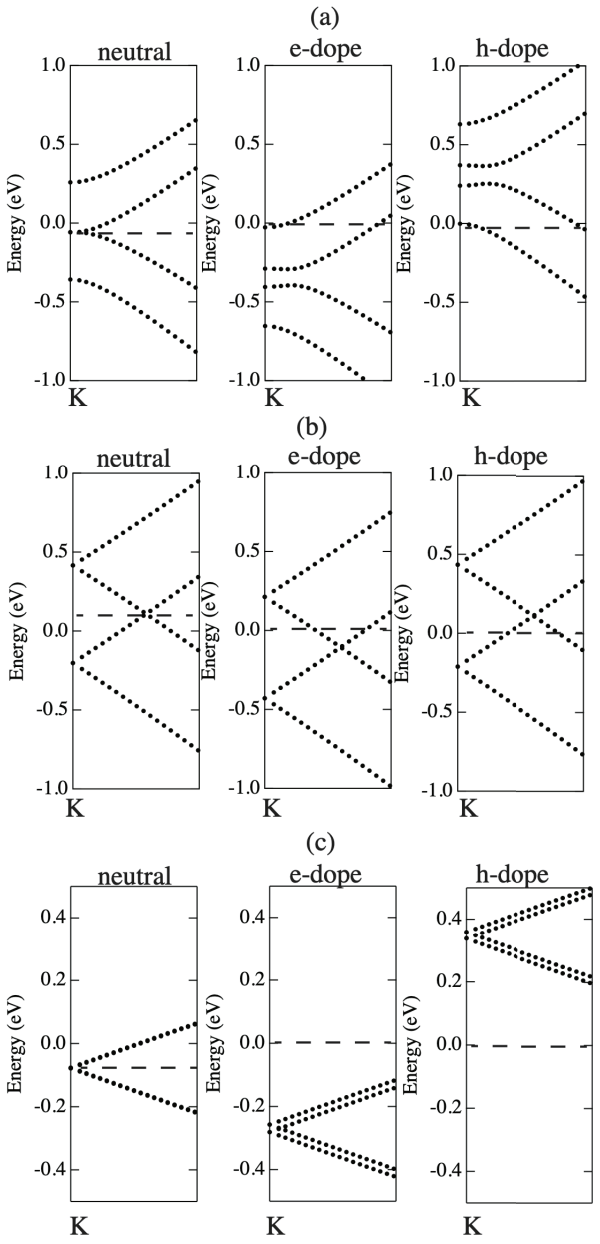

FIG. 5. Electronic energy band at the vicinity of the K point and around the Fermi level of the bilayer graphene with (a) AB, (b) AA, and (c) twisted interlayer arrangements, showing the energy band under neutral (left plots), electron doped (0.19e /nm^2) (center plots), and hole doped (0.19h /nm^2) (right plots) bilayer graphene. Horizontal dotted lines dente the Fermi level energy. The range of the horizontal axis corresponds to 20% of the K-Γ line.